Constructing Self-supported Pt/MoO$_2$ on Molybdenum Mesh for High-efficient Hydrogen Evolution Reaction

Jin Li,[a] Panpan Zhang,[a] Yunli Yang[a], Jian Zhang,[b] Meisa Zhou,[c] Heng Zhang,[d*] Guilong Liu,[a] Naiteng Wu,[a*] Changzhou Yuan,[e*] Xianming Liu[a*]

[a]College of Chemistry and Chemical Engineering, and Henan Key Laboratory of Function-Oriented Porous Materials, Luoyang Normal University, Luoyang 471934, P. R. China

[b]New Energy Technology Engineering Lab of Jiangsu Province, College of Science, Nanjing University of Posts & Telecommunications (NUPT), Nanjing 210023, P. R. China

[c]School of Materials Science and Engineering, University of Science and Technology Beijing, Beijing 100083, P. R. China

[d]Science Island Branch of Graduate School, University of Science and Technology of China, Hefei, 230026, P. R. China

[e]School of Materials Science & Engineering, University of Jinan, Jinan, 250022, P. R. China,

*Corresponding authors

1. Electrochemical measurements

In this research, the HER activity was examined using a standard three-electrode system with an electrochemical workstation (CHI760E) at room temperature. The experiments involved an electrode, prepared as earlier described, serving as the working electrode. A carbon rod and an Hg/Hg$_2$Cl$_2$ electrode were used as the counter and reference electrodes, respectively. Potentials were measured against the Hg/Hg$_2$Cl$_2$ reference and converted to the reversible hydrogen electrode (RHE) scale using the Nernst equation: $E_{RHE} = E_{(Hg/Hg2Cl2)} + 0.0591pH + 0.244$. All potentials mentioned in this study were adjusted for a 95% IR drop, except where noted otherwise. Before conducting electrochemical tests, the working electrode underwent activation and stabilization through 100 cyclic voltammetry (CV) cycles at a scan rate of 100 mV s^{-1}. Subsequently, the HER electrocatalytic efficiency was assessed using linear sweep voltammetry (LSV)

at a scan rate of 2 mV s^{-1} in a 0.5 M H$_2$SO$_4$ solution (pH 0.26). The Tafel slope was calculated from the LSV data. Additionally, prior to electrochemical measurements, the 0.5 M H$_2$SO$_4$ solution was saturated with argon gas. The double-layer capacitance, used to estimate the electrochemical active surface areas, was measured in the non-faradaic potential range (0.1-0.2 V vs. RHE) through CV at different scan rates. Electrochemical impedance spectroscopy tests were conducted at 20 mV overpotential over a frequency range from 100 kHz to 10 mHz, with an AC potential amplitude of 5 mV. The obtained results were analyzed using Zview software. The stability of the catalyst was evaluated through 5000 CV cycles, ranging from −0.1 to −0.6 V at a scan rate of 50 mV s^{-1}. Additionally, chronoamperometry tests were conducted at a 27 mV overpotential for a duration of 240 hours.

2. Materials Characterizations

To characterize the synthesized materials, various advanced techniques were employed. The morphological features were examined by field emission scanning electron microscope (FESEM, ZEISS-Merlin) with an integrated energy dispersive X-ray (EDX) mapping function, along with transmission electron microscope (TEM, JEOL, JEM-2100F). The crystal structures of the materials were scrutinized using X-ray diffraction (XRD, Bruker D8 advance) system. Additionally, surface chemical compositions were probed by X-ray photoelectron spectroscope (XPS, Perkin-Elmer Model PHI 5600), which features a monochromatic aluminum anode X-ray source and boasts a resolution range of 0.3-0.5 eV. To analyze the elemental composition of the catalyst samples, an inductively coupled plasma optical emission spectrometer (ICP-OES, iCAP 7600) was applied.

3. Computational calculations

Density functional theory calculations were conducted using the Dmol3 program package within the Materials Studio 2020 software. The Perdew-Burke-Ernzerhof function

of the generalized gradient approximation was employed to describe electron exchange and correlation. Computational parameters included a self-consistent field tolerance of 1.0×10^{-7} Ha per atom, an energy tolerance of 2.0×10^{-7} Ha per atom, a maximum force gradient of 0.002 Ha $Å^{-1}$, a maximum atomic displacement of 0.005 Å, an orbital cutoff of 4.6 Å, and thermal smearing of 0.005 Ha for rapid convergence.

Supercells for Pt and MoO_2 were modeled as $(6 \times 6 \times 2)$ (111) slabs and $(3 \times 3 \times 2)$ (011) slabs respectively. A 20 Å vacuum space was maintained as a periodic boundary condition. Pt clusters, each containing ten atoms, were adsorbed onto the MoO_2 supercells to form Pt/MoO_2 supercells. The Gibbs free energy change for hydrogen adsorption (ΔG_{H*}) was calculated using: $\Delta G_{H*} = E_{total} - E_{sur} - 1/2 E_{H2} + \Delta E_{ZPE} - T\Delta S$. In this equation, E_{total} is the total energy of the adsorption state, E_{sur} the energy of the unadorned surface, E_{H2} the total energy of H_2 gas, ΔE_{ZPE} the zero-point energy change, T the room temperature (298.15 K), and ΔS the entropy change. Based on previous report, $\Delta E_{ZPE} - T\Delta S$ is considered to be 0.24 eV, making the formula for ΔG_{H*} become: $\Delta G_{H*} = E_{total} - E_{sur} - 1/2 E_{H2} + 0.24$.
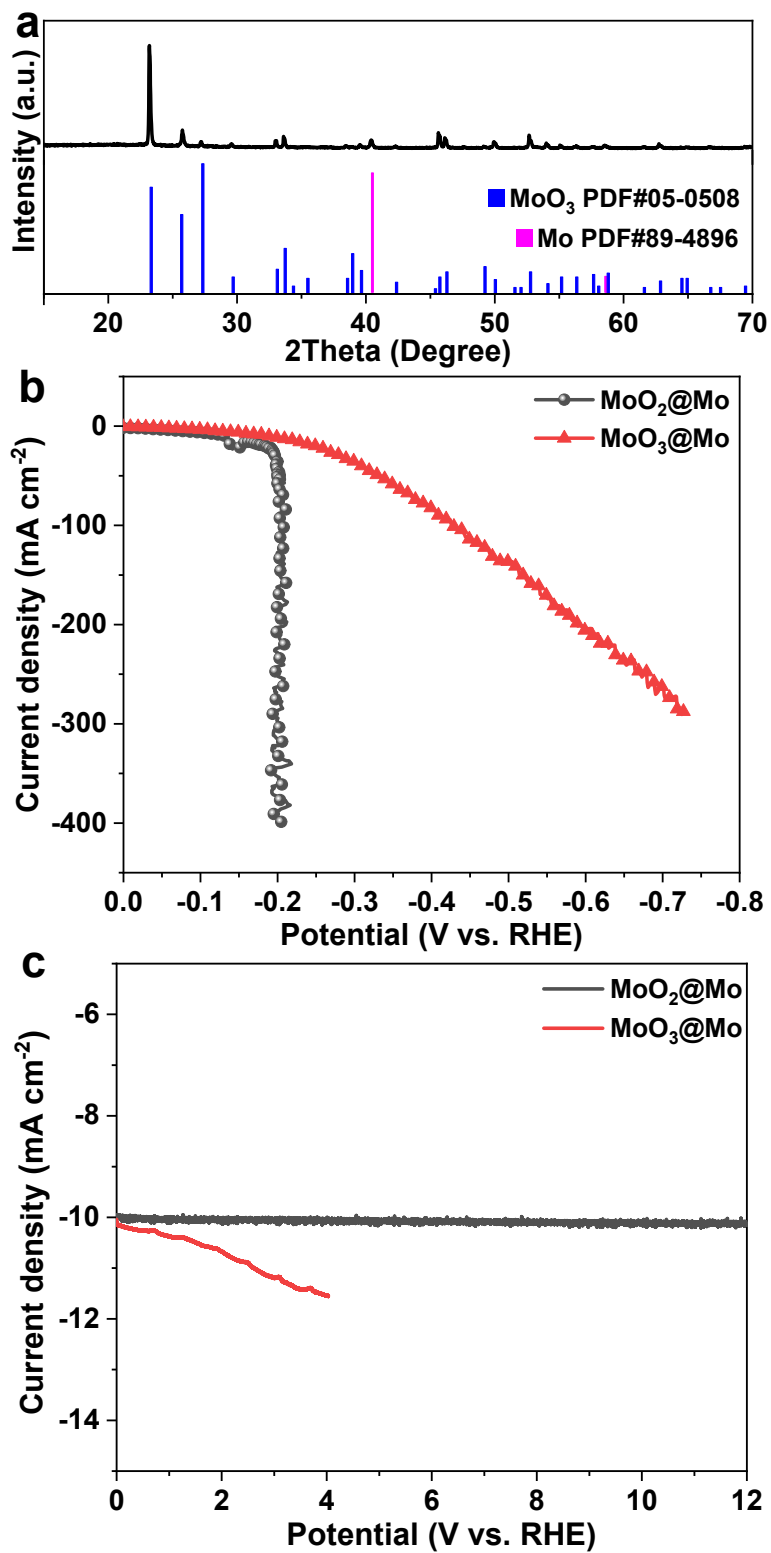
Figure S1. (a) XRD pattern of MoO$_3$@Mo. (b) LSV curves of MoO$_3$@Mo and MoO$_2$@Mo. (c) Chronoamperometry test of MoO$_3$@Mo and MoO$_2$@Mo.
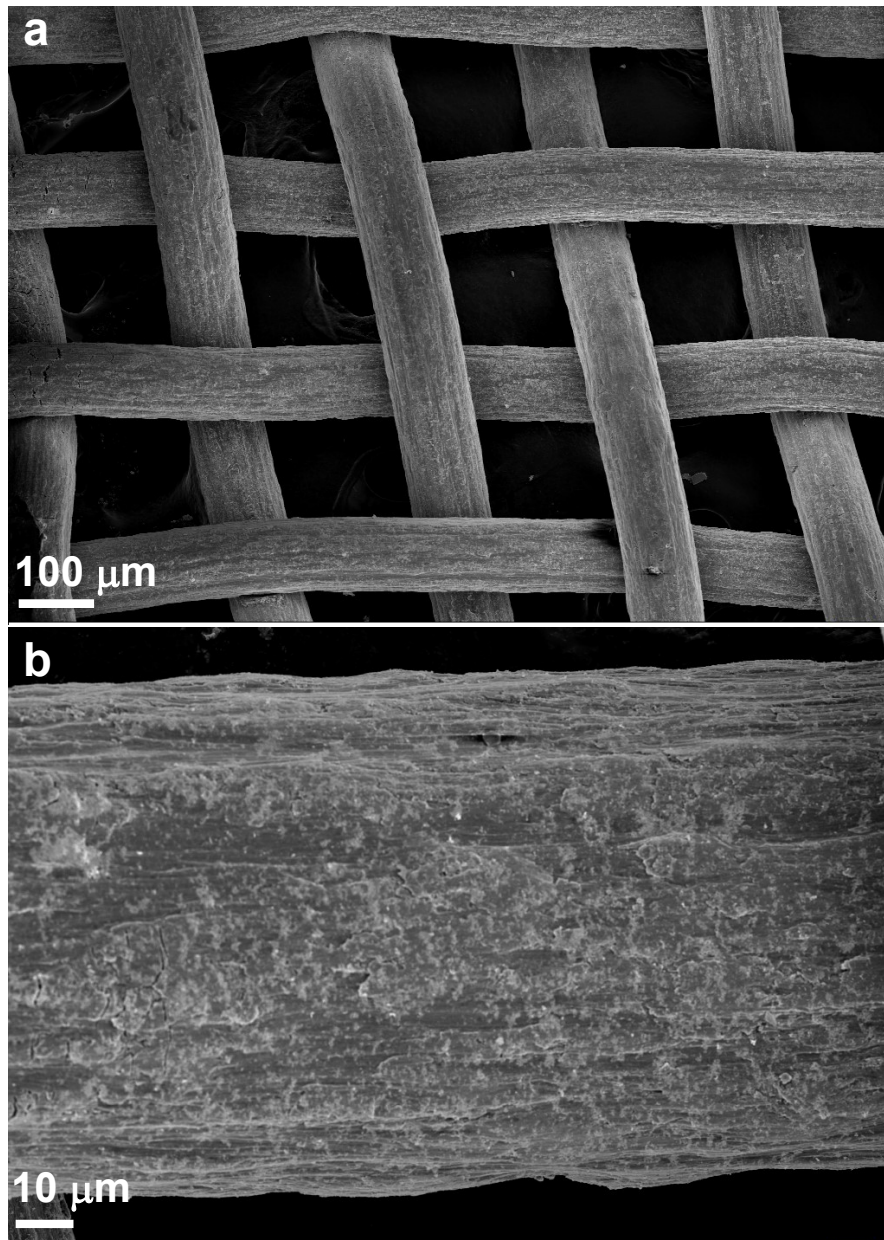
4

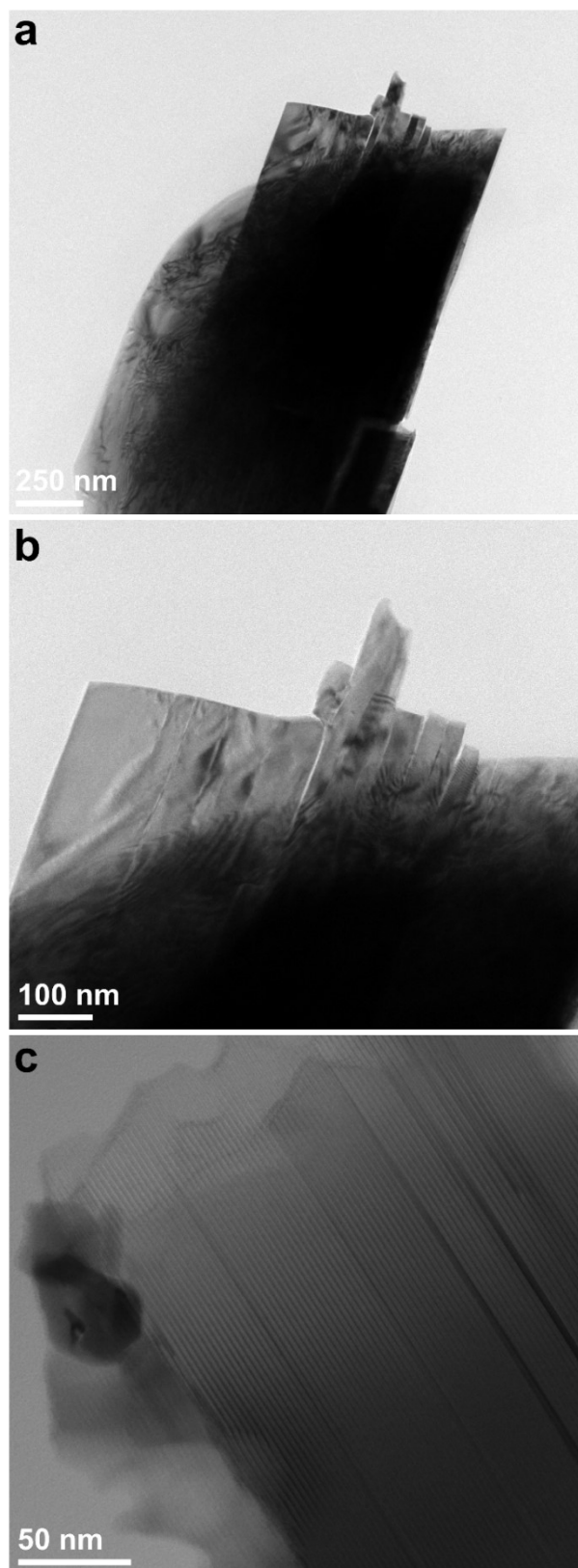**Figure S2.** FESEM images of the sample synthesized without KI.

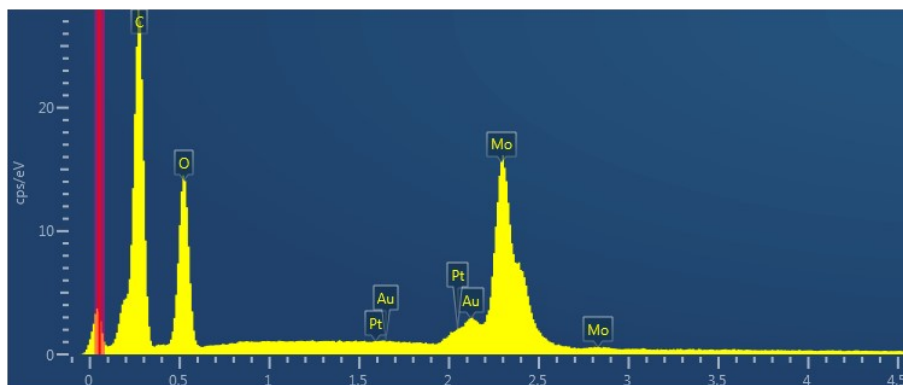**Figure S3.** TEM images of the Mo mesh treated by KI under air.
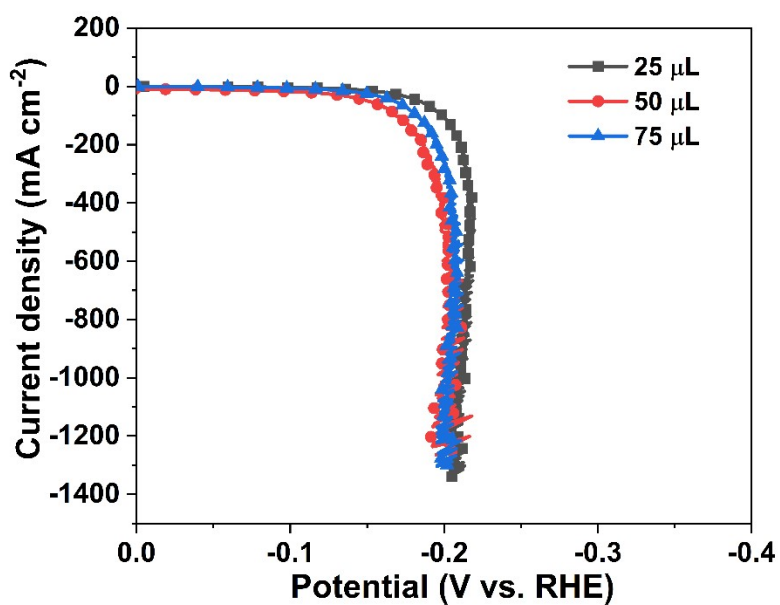
Figure S4. EDX image of Pt/MoO$_2$@Mo.

Figure S5. LSV curves of Pt/MoO$_2$@Mo with different contents of chloroplatinic acid.
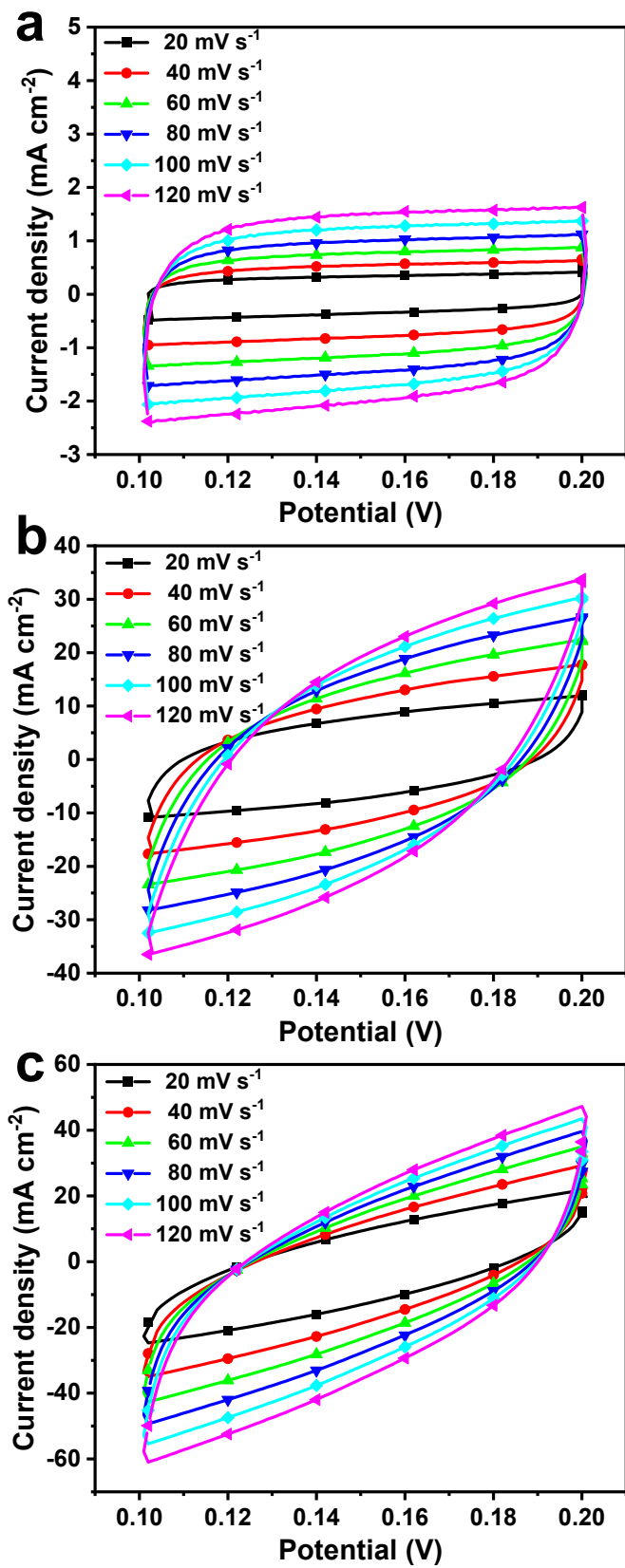
Figure S6. CV curves with different scan rates for (a) Pt@Mo, (b) MoO$_2$@Mo, and (c)
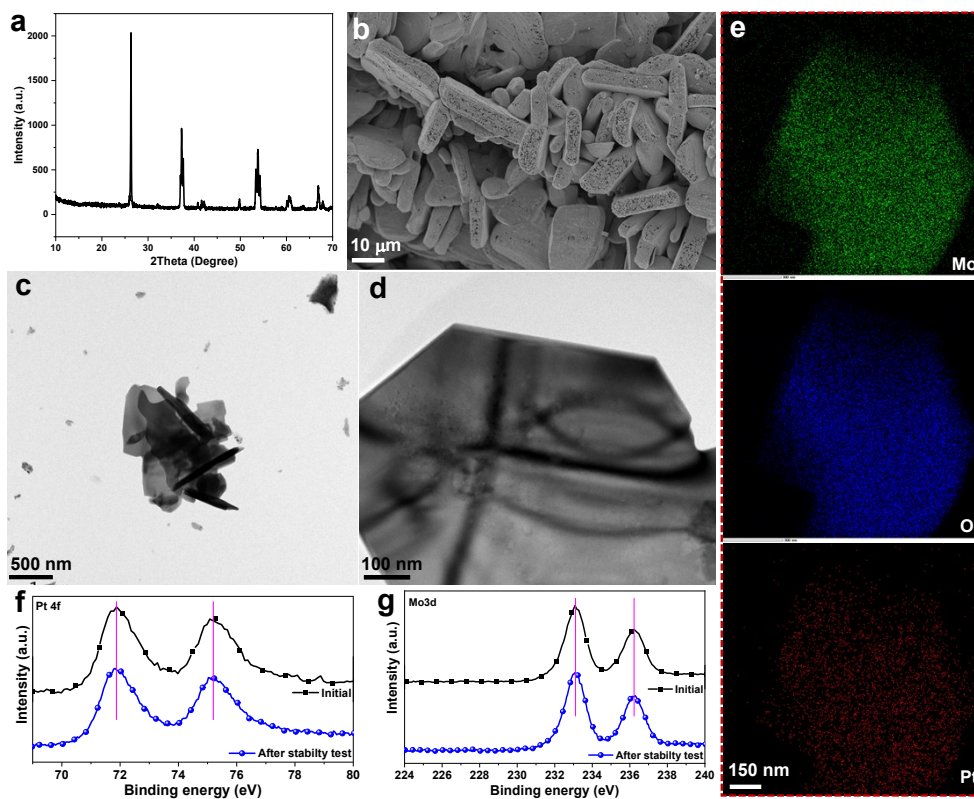
Pt/MoO$_2$@Mo.

Figure S7. (a) XRD pattern, (b) FESEM, and (c, d) TEM images of Pt/MoO$_2$@Mo after stability test. (e) EDX mapping images for Mo, O, and Pt after stability test. (f) Pt 4f, and (g) Mo3d XPS spectra of Pt/MoO$_2$@Mo before and after stability test.
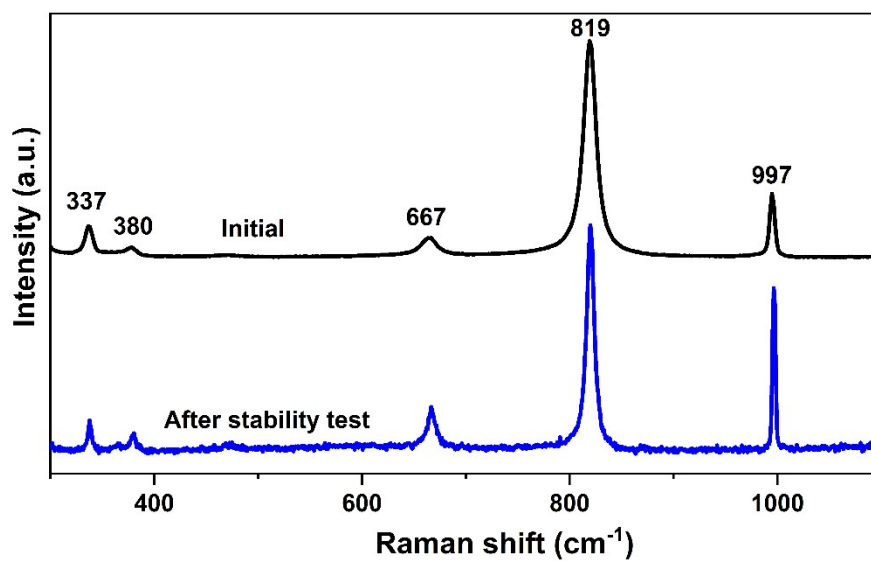

Figure S8. Raman spectra for Pt/MoO$_2$@Mo before and after stability test.

Raman spectroscopy was utilized to examine the alterations in Pt/MoO$_2$@Mo before and after stability assessment. The peaks observed at 667, 819, and 997 cm^{-1} are associated with the O-Mo bond vibrations of monoclinic phase MoO$_2$, while the peaks at 337 and 380 cm^{-1} correspond to phonon vibrations.[S1] These findings serve to reinforce the stability of the Pt/MoO$_2$@Mo electrode.
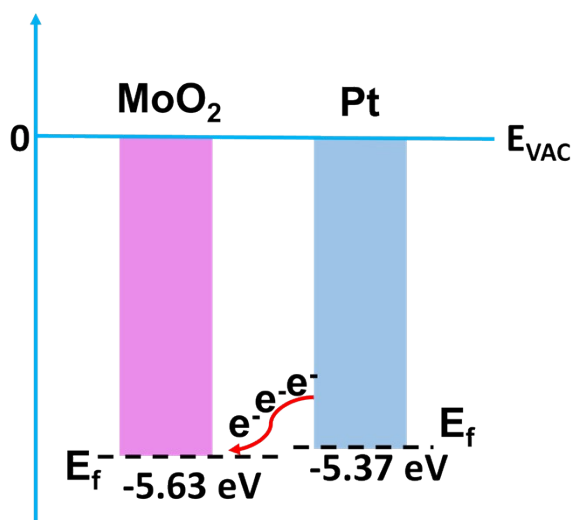

Figure S9. Energy band diagrams of MoO$_2$ and Pt, and the schematic illustrating of the electron transfer process between MoO$_2$ and Pt. E$_{VAC}$: Vacuum energy, E$_f$: Fermi level.

Table S1. The weight percentages of Pt contents in the Pt/MoO$_2$@Mo samples before and after stability test determined by ICP

Element	Before stability test	After stability test
Pt (wt%)	0.67%	0.62%

Table S2. Electrocatalytic HER parameters of Pt/MoO$_2$@Mo synthesized in this work and electrocatalysts reported previously at 10 mA cm^{-2} in 0.5 M H$_2$SO$_4$. These literatures relate to MoO$_2$ supports.

Catalysts	Pt loading content (wt%)	Overpotential (mV)	Tafel slope (mV dec^{-1})	Reference
Pt/MoO$_2$@Mo	0.67	26.8	59.2	This work
0.5 wt% Pt-MoO$_2$/MWCNTs	0.5	60	43	S2
Pt-MoO$_2$@PC	8.32	20	22	S3
Pt@MoO$_2$/MoS$_2$	/	42	26.6	S4
Pt@MoO$_2$/MoOC	/	98.99	81.4	S5
0.5 wt% Pt Cs/MoO$_2$ NSs-L	0.5	47	32.6	S6
1.1 wt% Pt SAs/MoO$_2$	1.1	9.3	28.78	S7
Pt/Ni-Mo-N-O	0.22	32	31.5	S8

References

S1.   Y. Mao, Y. Hu, J. Shen, R. Wang, H. Zhang, R. Wang, P. Zhao and B. Wang, *J. Alloys Compd.*, 2023, **960**, 170880.

S2.   X. Xie, Y.-F. Jiang, C.-Z. Yuan, N. Jiang, S.-J. Zhao, L. Jia and A.-W. Xu, *J. Phys. Chem. C*, 2017, **121**, 24979-24986.

S3.   Y. Jiang, M. Yang, M. Qu, Y. Wang, Z. Yang, Q. Feng, X. Deng, W. Shen, M. Li and R. He, *J. Mater. Chem. A*, 2020, **8**, 10409-10418.

S4.   B. Dong, Y.-N. Zhou, J.-C. Zhou, Y. Ma, N. Yu, R.-N. Luan, Y.-W. Dong and Y.-M.

Chai, *Fuel*, 2022, **324**, 124343.

S5.   S. Li, J. Liang, X. Tan, F. Li, X. Wang, L. Ma, L. Zhang and K. Cheng, *Int. J. Hydrogen Energy*, 2024, **51**, 1128-1137.

S6.   X. Li, J. Yu, J. Jia, A. Wang, L. Zhao, T. Xiong, H. Liu and W. Zhou, *Nano Energy*, 2019, **62**, 127-135.

S7.   Y. Qiu, S. Liu, C. Wei, J. Fan, H. Yao, L. Dai, G. Wang, H. Li, B. Su and X. Guo, *Chem. Eng. J.*, 2022, **427**, 131309.

S8.   W. Yu, Z. Chen, Y. Fu, W. Xiao, B. Dong, Y. Chai, Z. Wu and L. Wang, *Adv. Funct. Mater.*, 2022, **33**, 2210855.